# Supplementary Information
# Natural Organic Matter Surface Coverage as a Predictor of Heteroaggregation between Nanoparticles and Colloids

Dylan M. Oney[1,2] and Jeffrey A. Nason[1*]

* Corresponding Author: jeff.nason@oregonstate.edu

[1] School of Chemical, Biological and Environmental Engineering, Oregon State University, 116 Johnson Hall, 105 SW 26th St., Corvallis, OR 97331

[2] Current Address: US Army Corps of Engineers, Tulsa District, 2488 E 81st St. Tulsa, OK 74137

## Contents

## 1. Glass bead washing

Glass beads were washed in a manner similar to previously established procedures.[1] Briefly, glass beads were mixed in distilled, deionized (DDI) water, allowed to settle, and the water decanted; this process was repeated several times. The beads were then mixed in a 0.1 M sodium hydroxide solution, allowed to settle, and rinsed as above. This was repeated with a 0.1 M hydrochloric solution and then a 10% sulfuric acid solution. Finally, the beads were rinsed at least 5 times with DDI water. The beads were then dried at 98°C overnight.

## 2. Nanoparticle homoaggregation

An example time resolved dynamic light scattering experiment for bPEI-AuNPs in the presence of SRNOM is shown in Figure S1. The extent of aggregation ($D_{h,15}/D_{h,0}$) is calculated by normalizing the size measured at 15 minutes (average of the five readings leading up to 15 minutes) by the initial size.

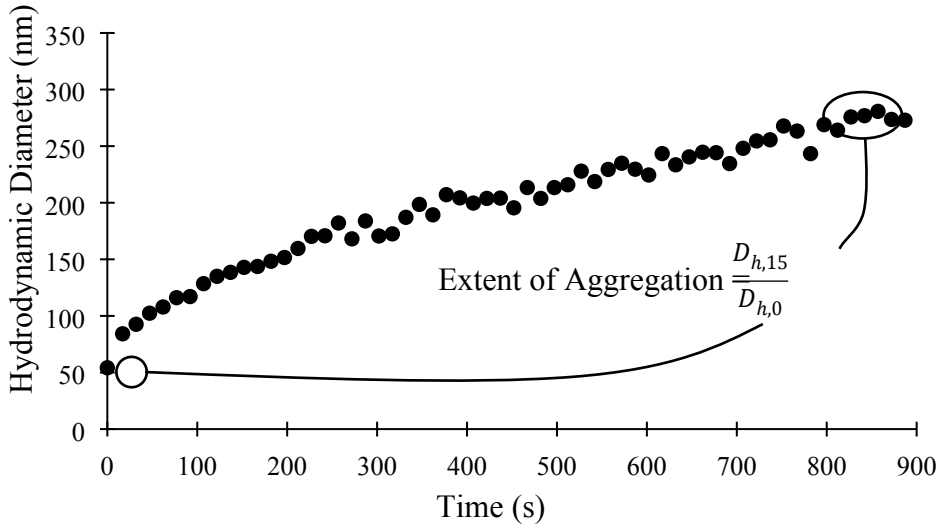


**Figure S1.** Change in hydrodynamic diameter over time. 2 mg/L bPEI-AuNPs, 1 mM HEPES, 20 mM NaCl, 0.3 mg C/L SRNOM.

## 3. Estimation of SRNOM surface coverage on bPEI-AuNPs

Changes in the electrophoretic mobility were used as a surrogate for SRNOM adsorption and thus $\theta_{ENP}$. According to Smoluchowski's mobility equation (Eq. S1), electrophoretic mobility is proportional to zeta potential (a close approximation of the surface charge).

$$\mu = \frac{\varepsilon_r \varepsilon_0}{\eta} \zeta \tag{S1}$$

Where $\mu$ is the electrophoretic mobility; $\varepsilon_r$ is the relative permittivity of the electrolyte solution; $\varepsilon_0$ is the permittivity of a vacuum; $\eta$ is the viscosity of the electrolyte solution; and $\zeta$ is the zeta potential. At the conditions of this work the $\kappa a > 14$.

It was assumed that adsorption of SRNOM would directly impact $\zeta$ and thus $\mu$. The mobility of the bPEI-AuNPs at each SRNOM concentration was subtracted from the mobility of the bPEI-AuNPs in the salt/buffer matrix without SRNOM present. This change in mobility was used to estimate surface coverage of SRNOM on the nanoparticles by fitting a Langmuir isotherm (Eq. S3) to the data as follows:

$$\text{assume } \left(\mu_{DOM=0} - \mu_{DOM=x}\right) \propto \left(\zeta_{DOM=0} - \zeta_{DOM=x}\right) \propto q \tag{S2}$$

$$\theta_{ENP} = \frac{q}{q_{\max}} = \frac{KC}{1+KC} \tag{S3}$$

Where $q$ is the adsorption density of DOM on the AuNP surface; $q_{max}$ is the maximum adsorption density; $K$ is the Langmuir adsorption constant; and $C$ is the solution phase DOM concentration (here normalized by the bPEI-AuNP concentration in units of mg C/m$^2$ ENPs).

Calculations assumed that DOM adsorption does not significantly deplete solution phase DOM concentration. Values of $K$ (0.09 m$^2$/mg C) and $\left(\mu_{DOM=0} - \mu_{DOM=x}\right)_{\max}$ (2.13 μm·cm·V$^{-1}$·s$^{-1}$) were determined by a non-linear least squares fit to the experimental data shown in Figure 2b of the main text and $\theta_{ENP}$ calculated as shown in Eq. S4. Table S1 shows example calculations.

$$\theta_{ENP} = \frac{\left(\mu_{DOM=0} - \mu_{DOM=x}\right)}{2.13} = \frac{0.09C}{1+0.09C} \tag{S4}$$

**Table S1.** Example calculation of the change in electrophoretic mobility used to estimate NP surface coverage.

| SRNOM Conc. | ENP Conc. | DOM:ENP | μ | $\mu_{DOM=0} - \mu_{DOM=x}$ | | $\theta_{ENP}$ |
|---|---|---|---|---|---|---|
| (mg C/L) | (mg Au/L) | (mg C/m$^2$) | (μm·cm·V$^{-1}$·s$^{-1}$) | (μm·cm·V$^{-1}$·s$^{-1}$) | | (-) |
| 0 | 5 | 0 | 0.83 | 0.83−0.83= | 0 | 0 |
| 0.15 | 5 | 5.79 | 0.15 | 0.83−0.15= | 0.68 | 0.32 |
| 3 | 5 | 115.8 | -1.20 | 0.83−(−1.20)= | 2.03 | 0.93 |

Experimental data from Gonzalez et al.[2] was used to validate this method of estimating SRNOM adsorption onto the bPEI-AuNPs. The authors measured the solution depletion of dodecyl sulphonate due to adsorption onto polystyrene particles. From this, adsorption isotherms were calculated, and fractional coverage was estimated as $q/q_{max}$. The authors also measured the electrophoretic mobility of the polystyrene particles after exposure to the dodecyl sulphonate. The fractional coverage as determined using the adsorption isotherm and as determined using the change in electrophoretic mobility were quite similar (Figure S2). The agreement in surface coverage determined by these two methods suggest that the change in electrophoretic mobility can be used as a surrogate for the adsorption of charged macromolecules.

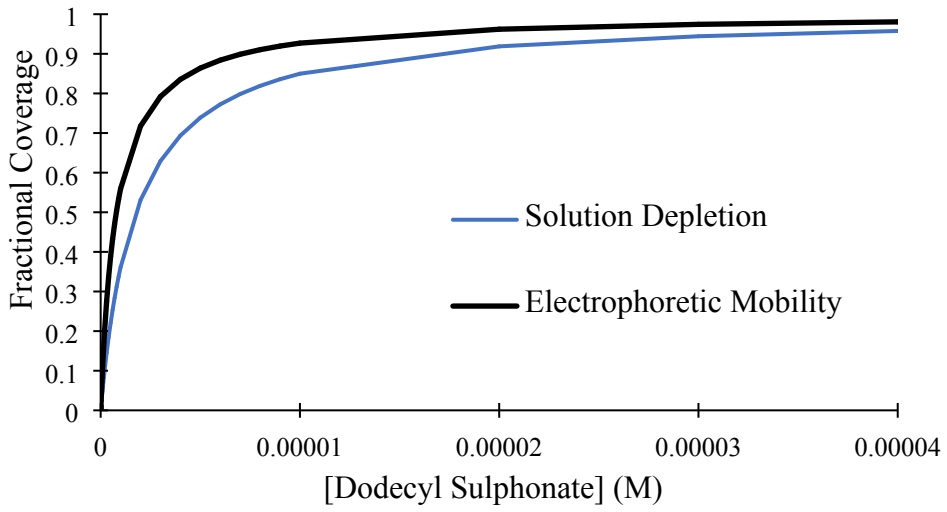


**Figure S2.** Fractional coverage of dodecyl sulphonate on polystyrene particles estimated by the change in electrophoretic mobility and solution depletion using the data of Gonzalez et al.[2]

## 4. Gold nanoparticle concentration determination

A standard curve was developed by plotting absorbance at the surface plasmon resonance peak (535 nm) vs. gold nanoparticle concentration (Figure S3). Absorbance was corrected by subtracting the absorbance of a blank containing the same aquatic medium, but no nanoparticles. For all collected samples, absorbance was recorded at wavelengths from 400-900 nm to and Nanoparticle concentration was determined by measuring the absorbance of collected samples from mixed batch experiments after glass beads had settled.

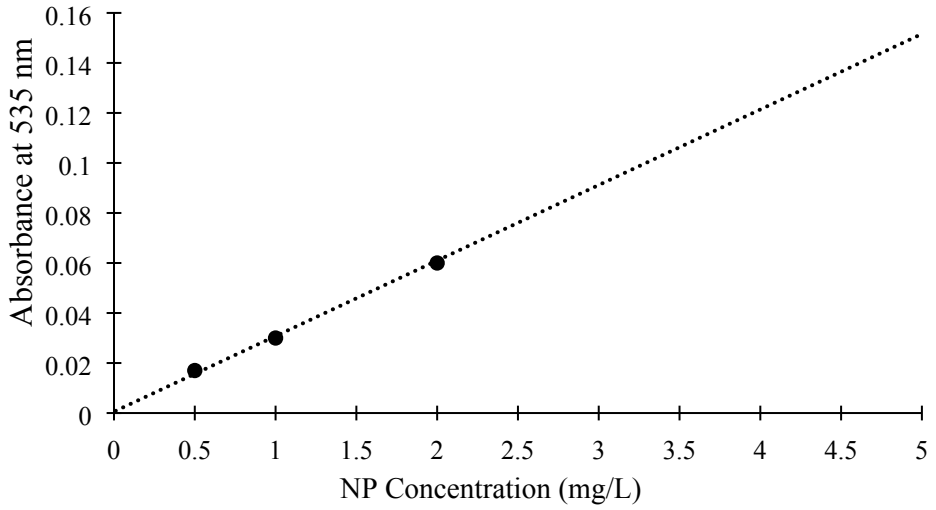


**Figure S3.** Background corrected bPEI-AuNP absorbance-concentration standard curve

## 5. Suspended Particle Mixing Experiments

A schematic of the experimental steps involved with the suspended particle mixing experiments is shown in Figure S4.

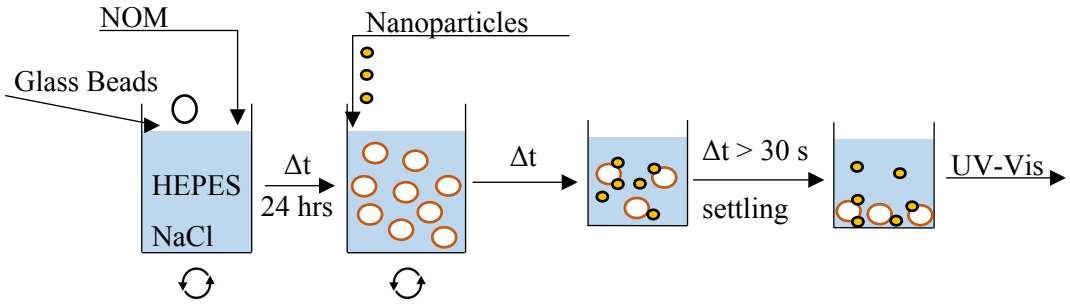


**Figure S4.** Schematic of the experimental protocol used for batch suspended particle mixing experiments

## 6. Analysis of batch suspended particle mixing experiments

Background-corrected absorbance spectra from an example experiment are shown in Figure S5. Full spectra were collected as a means of detecting nanoparticle homoaggregation during experiments. The absorbance at the surface plasmon resonance peak (535 nm) was used to determine the concentration of remaining AuNPs in suspension as described above. Nanoparticle concentration for this same experiment is plotted as a function of time in Figure S6. Finally, data were transformed and the quantity $\ln(N_0/N_t)$ was plotted as a function of time. The slope of the linear portion of the resulting data (6-7 data points) was calculated using linear regression to yield the pseudo first order rate constant $\alpha\beta B$ (Figure S7). The last point in a given trial was omitted if its inclusion resulted in a reduction in the $R^2$ value (as shown in Figure S7).

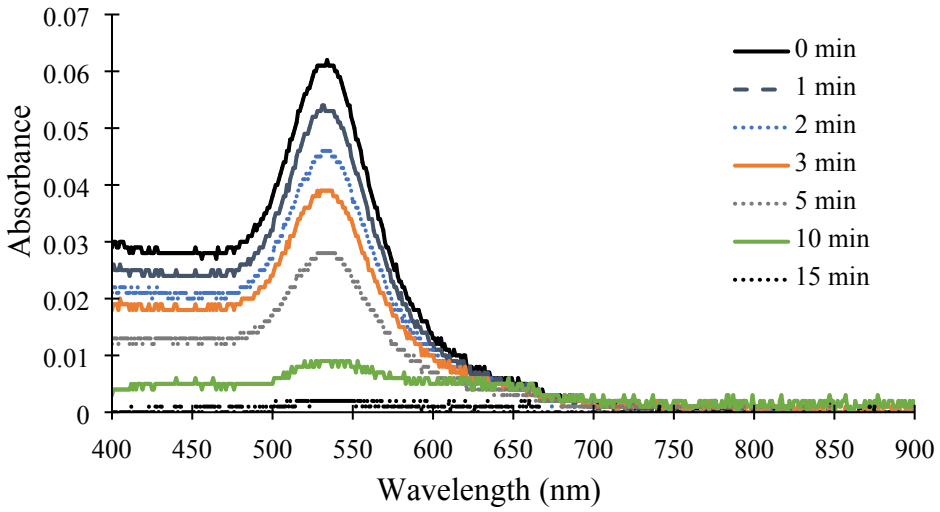


**Figure S5.** Background corrected UV-Vis spectra obtained from a batch suspended particle mixing experiment with 2 mg/L bPEI-AuNPs and 15 g/L glass beads.

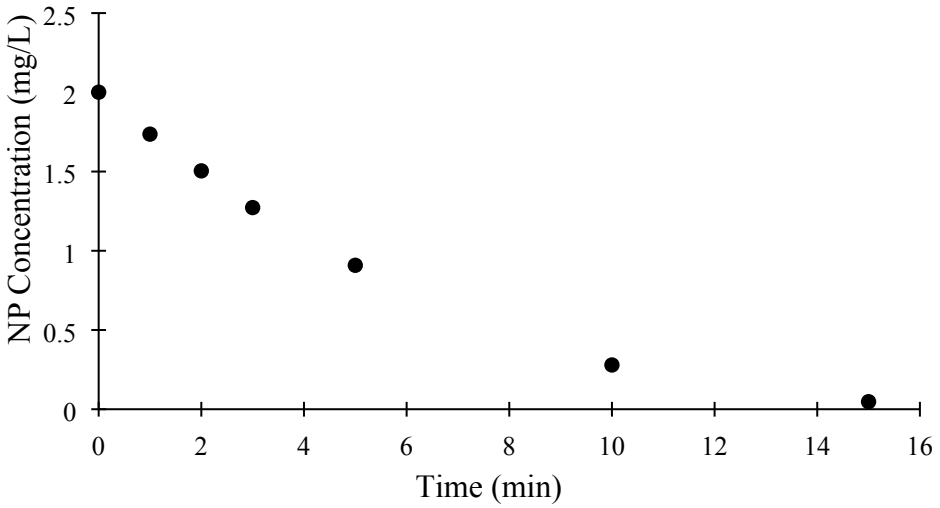


**Figure S6.** Nanoparticle concentration as a function of time during a batch suspended particle mixing experiment with 2 mg/L bPEI-AuNPs and 15 g/L glass beads

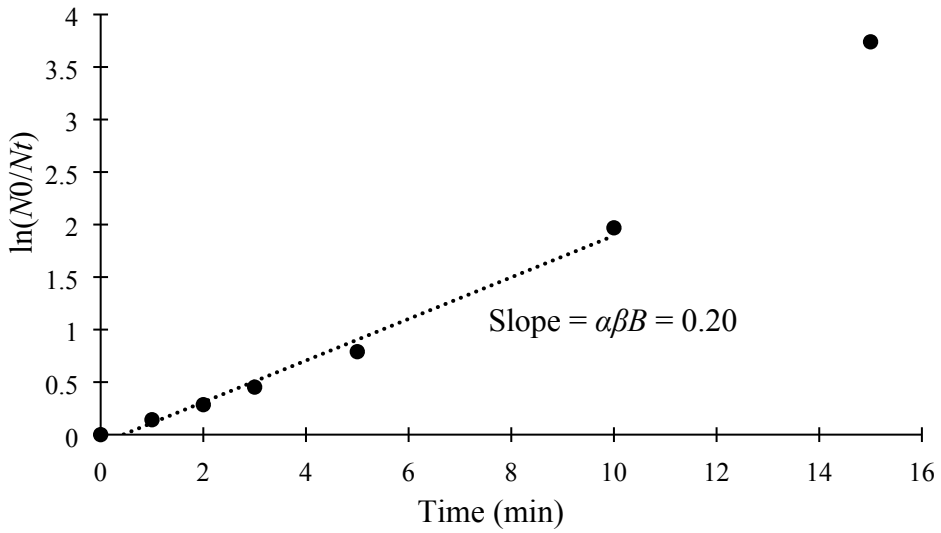


**Figure S7.** Transformed nanoparticle concentration data from a batch suspended particle mixing experiment with 2 mg/L bPEI-AuNPs and 15 g/L glass beads. The slope of the best fit line is the pseudo first order rate constant $\alpha\beta B$. The data point at 15 min was omitted from the slope calculation as its inclusion reduced the $R^2$ value.

## 7. Comparison of bPEI-AuNP homoaggregation with previous work

Figure S8 compares the extent of aggregation for 60 nm bPEI-AuNPs in the presence of SRNOM from this study with the results of Surette and Nason[3] using 12 nm bPEI-AuNPs. The same trend in aggregation is observed, with the maximum extent of aggregation occurring at nearly the same DOM:ENP ratio in both cases.

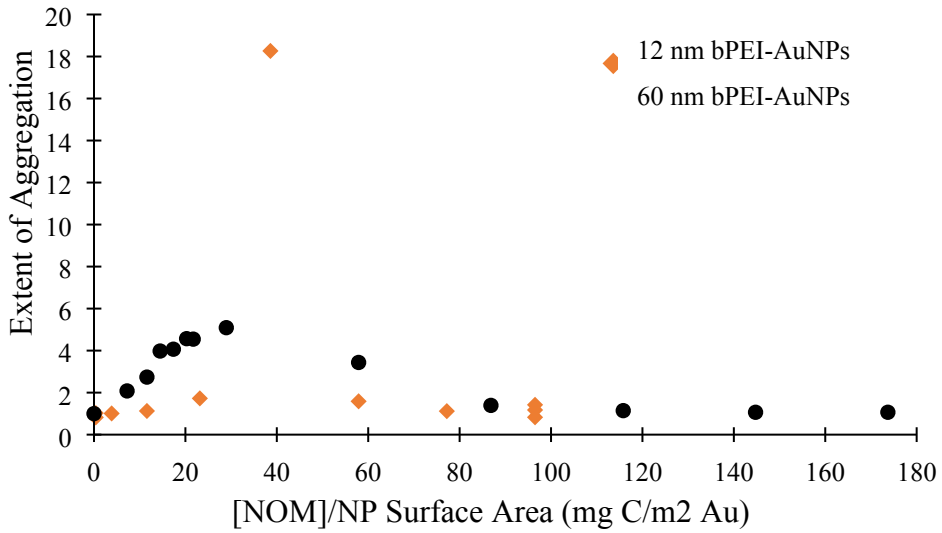


**Figure S8.** Extent of homoaggregation of bPEI-AuNPs in the presence of SRNOM. Data with 12 nm bPEI-AuNPs were collected using 1 mg/L NP, 1 mM KCl, and varying concentrations of SRNOM. pH was adjusted with KOH.[3] Data with 60 nm bPEI-AuNPs were collected using 2 mg/L NP, 20 mM NaCl, 1 mM HEPES, and varying concentrations of SRNOM.

## 8. Adsorption of SRNOM to glass beads

Adsorption experiments consisted of samples with and without glass beads so as to account for any SRNOM loss to the reaction vessels (polyethylene centrifuge tubes). Methods blanks containing the same aquatic matrix (10 mM sodium bicarbonate and 10 mM sodium chloride) but no glass beads were also performed. Background TOC measured in samples with no added SRNOM were subtracted from measured total organic carbon (TOC) concentrations in samples with added SRNOM. The background corrected TOC content measured after 24 hours in samples without GBs was not significantly different from the TOC in samples with GBs for a given SRNOM concentration (Figure S9). This indicates that there was negligible SRNOM adsorption by the GBs. Adsorption of SRNOM onto soda-lime glass was also examined using quartz crystal microbalance with dissipation monitoring using a soda-lime glass sensor (Figure S10). Minimal changes in the frequency of the third overtone validates that SRNOM does

not adsorb to the soda-lime glass to significant extent under the conditions of these experiments.

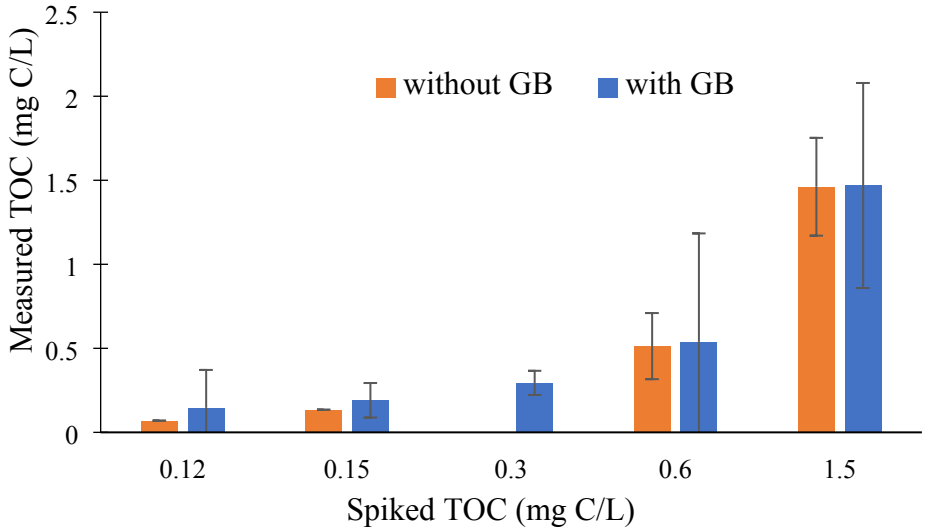


**Figure S9.** Average measured TOC in samples with and without glass beads. Error bars represent 95% confidence intervals.

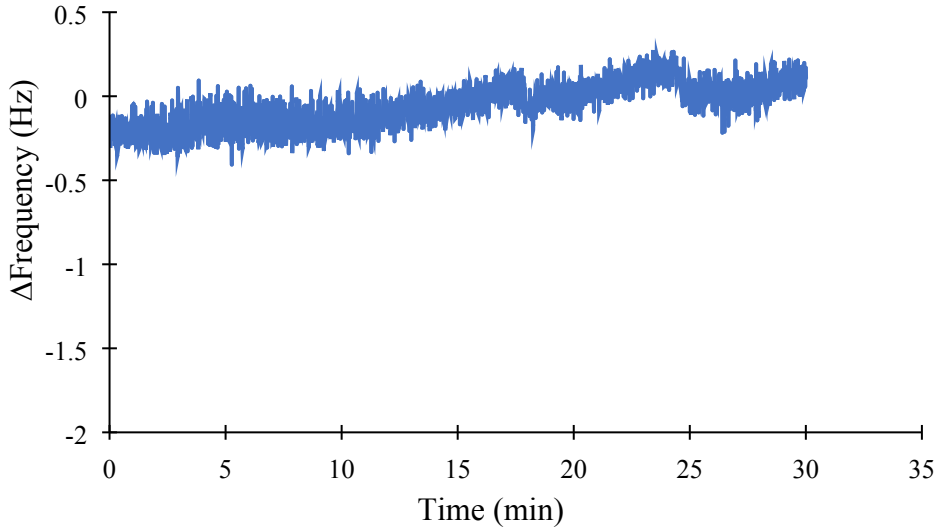


**Figure S10.** Quartz crystal microbalance with dissipation monitoring validation of minimal SRNOM adsorption to a soda lime glass sensor.

## 9. Heteroaggregation of bPEI AuNPs with glass beads

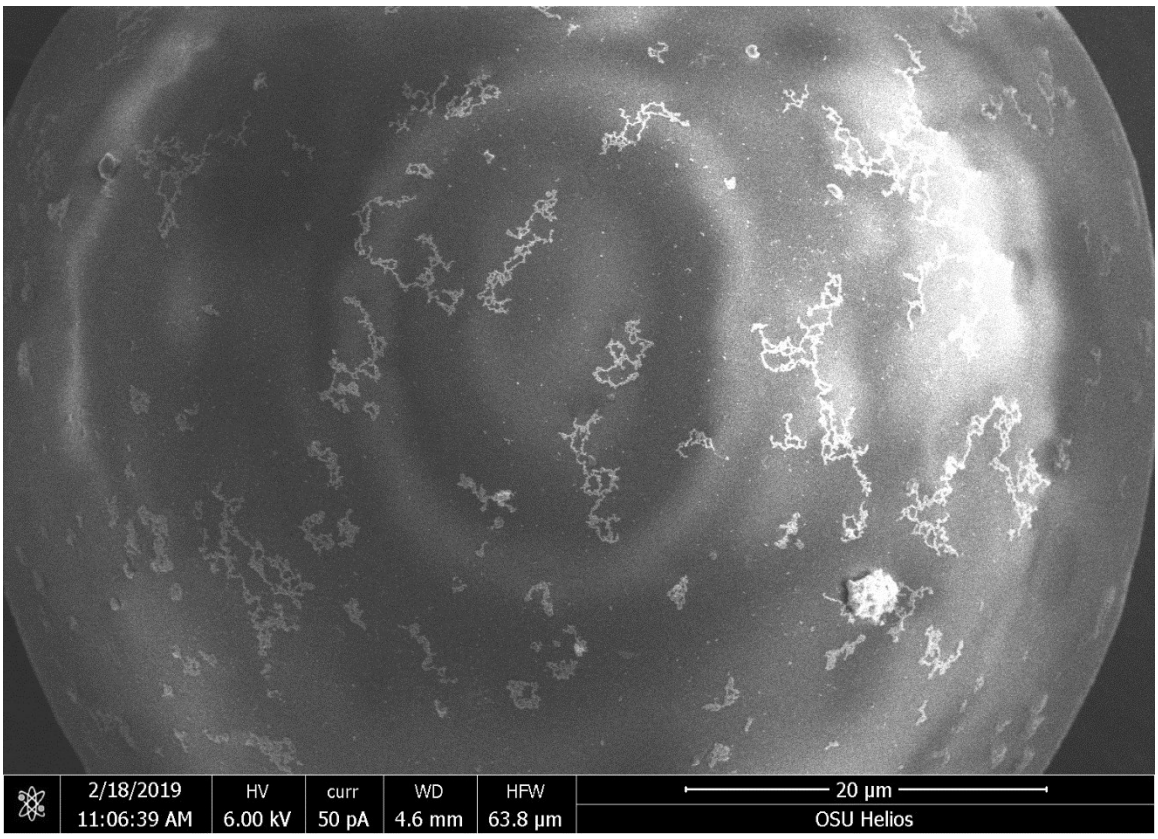


**Figure S11.** Scanning electron microscopy image of bPEI-AuNP attachment to a glass bead. Both individual bPEI-AuNPs and AuNP aggregates are visible on the glass bead surface. It is unclear whether bPEI-AuNPs attached in this aggregated state, or whether the drying and preparation process led to clustering of the bPEI-AuNPs. However, DLS and UV-vis measurements during this trial did not indicate that the bPEI-AuNPs were aggregating in suspension.

## 10. The impact of ENP homoaggregation on measured rate constants

The influence of ENP homoaggregation on the calculation of removal rates was evaluated by measuring ENP loss in the absence of GBs. The UV-Vis spectra from samples collected immediately after ENP addition (Figure S12) reveal that homoaggregation did occur for certain NOM:ENP ratios, consistent with the DLS results presented in Figure 2c in the main text. The quenching of the surface plasmon resonance peak and the formation of a shoulder at higher wavelengths are both indications of homoaggregation.[4] However,

the shape of the spectra obtained for a given set of conditions does not change over time (Figure S13), indicating that the homoaggregation state of the ENPs remained constant throughout the tests. This analysis illustrates the value of measuring absorbance spectra as opposed to absorbance at a single wavelength.

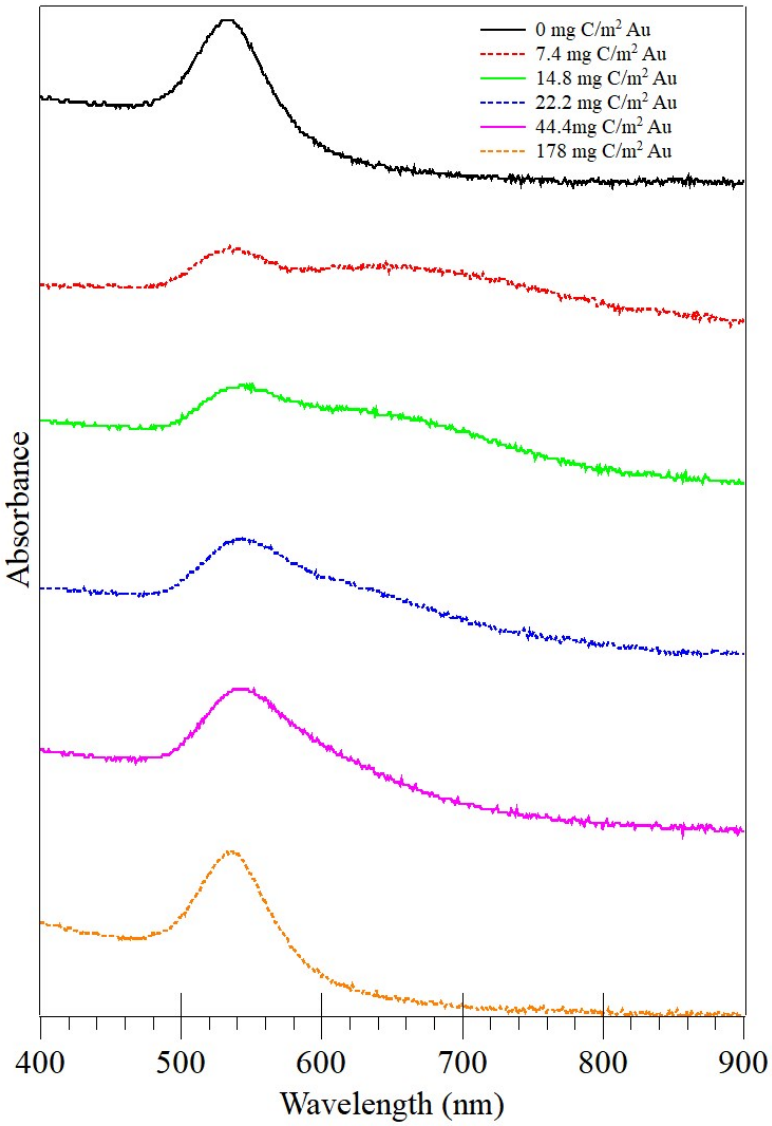


**Figure S12.** Initial spectra (t ≈ 0) for 2 mg/L bPEI-AuNPs, 20 mM NaCl, 1 mM HEPES, 0 g/L GB, and varying SRNOM concentrations.

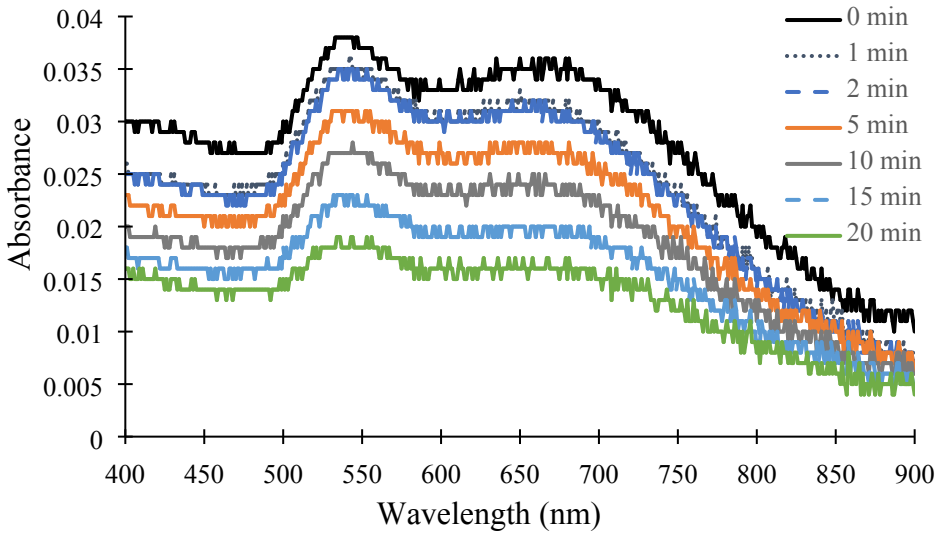


**Figure S13.** Background corrected UV-VIS spectra over time for 2 mg/L bPEI-AuNPs, 0 g/L GB, 20 mM NaCl, 1 mM HEPES, 0.15 mg C/L SRNOM.

The second potential effect of homoaggregation on the measured rate constants is the impact of an increase in ENP size on the collision frequency, $\beta$. The collision frequencies with short range adjustment factors described by Benjamin and Lawler[5] for 60 and 300 nm NPs colliding with 70 µm GBs are 1.88 x $10^{-5}$ and 1.89 x $10^{-5}$ $cm^3/s$, respectively. Calculations are shown below. This negligible influence of ENP size indicates that homoaggregation will not significantly affect $\beta$ or the calculated removal rates. Turner et al.[6] reached the same conclusion for collisions between 10-13 nm gold nanoparticles and soil.

The equations used for the calculation of $\beta$ are shown below. Table S2 shows the values used to calculate the collision frequencies and associated short range correction factors for the 61 nm bPEI-AuNPs and 70 µm GBs.[5]

$$\beta_{ij}^{tot} = \alpha_{ij}^{Br}\beta_{ij}^{Br} + \alpha_{ij}^{Sh}\beta_{ij}^{Sh} + \alpha_{ij}^{Sh}\beta_{ij}^{Sh} \quad \text{(S5)}$$

$$\beta_{ij}^{Br} = \frac{2k_BT}{3\mu}\left(\frac{1}{d_i} + \frac{1}{d_j}\right)\left(d_i + d_j\right) \quad \text{(S6)}$$

$$\beta_{ij}^{Sh} = \frac{1}{6} G \left( d_i + d_j \right)^3 \tag{S7}$$

$$\beta_{ij}^{DS} = \left| v_i - v_j \right| \frac{\pi}{4} \left( d_i + d_j \right)^2 \tag{S8}$$

$$\alpha_{ij}^{Br} = a + b\lambda + c\lambda^2 + d\lambda^3 \tag{S9}$$

$$\alpha_{ij}^{Sh} = \frac{8}{\left(1+\lambda\right)^3} 10^{a+b\lambda+c\lambda^2+d\lambda^3} \tag{S10}$$

$$\alpha_{ij}^{DS} = 10^{a+b\lambda+c\lambda^2+d\lambda^3} \tag{S11}$$

$$H_A = \frac{A}{18\pi\mu \left( d_j \right)^3 G} \tag{S12}$$

$$N_g = \frac{48A}{\pi \left( \rho_j - \rho_l \right) g \left( d_j \right)^4} \tag{S13}$$

For all mechanisms, linear interpolation was used to find values of *a*, *b*, *c*, and *d* that lie between those tabulated.

**Table S2.** Description and value of variables used to calculate collision frequencies and short-range correction factors.

| Variable | Description | Value |
|---|---|---|
| $k_B$ | Boltzman constant | 1.38 x $10^{-16}$ g·cm$^2$/s$^2$·K |
| $T$ | Temperature | 298 K |
| $\mu$ | Dynamic viscosity | 0.0089 g/cm·s |
| $d_i$ | NP diameter | 61 nm |
| $d_j$ | GB diameter | 70 µm |
| $\rho_j$ | GB density | 2.5 g/cm$^3$ |
| $\rho_l$ | Fluid density | 0.997 g/cm$^3$ |
| $g$ | Acceleration due to gravity | 9.81 m/s$^2$ |
| $A$ | Hamaker constant | 2.7 x $10^{-13}$ s$^2$/g·cm$^2$ |

| Variable | Description | Value |
|---|---|---|
| $\beta_{ij}^{Br}$ | Collision frequency due to Brownian motion | 3.5 x $10^{-9}$ $cm^3/s$ |
| $G$ | Shear rate | 23.8 $s^{-1}$ |
| $\beta_{ij}^{Sh}$ | Collision frequency due to fluid shear | 1.4 x $10^{-6}$ $cm^3/s$ |
| $v_i$ | NP settling velocity | 4.2 x $10^{-6}$ cm/s |
| $v_j$ | GB settling velocity | 0.45 cm/s |
| $\beta_{ij}^{DS}$ | Collision frequency due to differential settling | 1.7 x $10^{-5}$ $cm^3/s$ |
| $\lambda$ | Particle size ratio | 8.7 x $10^{-4}$ |
| $H_A$ | Dimensionless number characterizing collisions by fluid shear | 6.6 x $10^{-8}$ |
| $N_g$ | Dimensionless number characterizing collisions by differential sedimentation | 1.2 x $10^{-6}$ |
| $a_{Br}$ | | 0.871 |
| $b_{Br}$ | | -1.739 |
| $c_{Br}$ | | 2.371 |
| $d_{Br}$ | | -1.09 |
| $a_{Sh}$ | | -8.94 |
| $b_{Sh}$ | | 26.56 |
| $c_{Sh}$ | | -31.6 |
| $d_{Sh}$ | | 12.91 |
| $a_{DS}$ | | -3.01 |
| $b_{DS}$ | | 4.61 |
| $c_{DS}$ | | -6.88 |
| $d_{DS}$ | | 3.52 |
| $\alpha_{ij}^{Br}$ | Brownian motion correction factor | 0.87 |
| $\alpha_{ij}^{Sh}$ | Fluid shear correction factor | 9.5 x $10^{-9}$ |
| $\alpha_{ij}^{DS}$ | Differential settling correction factor | 8.7 x $10^{-4}$ |

Lastly, homoaggregation has the potential to increase the apparent removal rate *via* settling of larger homoaggregates. Stokes Law (Eq. S14) was used to calculate the settling velocity of the aggregated ENPs.[5]

$$v = \frac{2\left(\rho_p - \rho_f\right)g\left(r_p\right)^2}{9\mu} \quad \text{(S14)}$$

$v$ is the particle settling velocity; $\rho_p$ is the particle density (19.3 g/mL); $\rho_f$ is the fluid density (1 g/mL); $g$ is acceleration due to gravity (9.81 m/s$^2$); $r_p$ is the particle radius (150 nm); $\mu$ is the fluid viscosity (1 cP). A radius of 150 nm was chosen to represent the scenario of maximum aggregation seen in TR-DLS tests. The terminal settling velocity of ENP aggregates is 0.32 cm/hr which is not sufficient to account for ENP loss during the time between sample collection and analysis by UV-Vis. At most, the elapsed time was 40 minutes.

## 11. Rate constants for heteroaggregation depend on DOM:ENP ratio

Data from Figure 4 of the main text are presented here as a function of DOM concentration (*i.e.*, without accounting for differences in the DOM:ENP ratio). Measured rate constants for experiments using 5 mg/L bPEI-AuNPs are greater than those measured in experiments using 2 mg/L bPEI-AuNPs at the same DOM concentration due to the differences in $\theta_{ENP}$. At a given DOM concentration, a smaller fraction of the ENP surfaces are coated by DOM in experiments using the higher ENP concentration leading to higher attachment efficiencies.

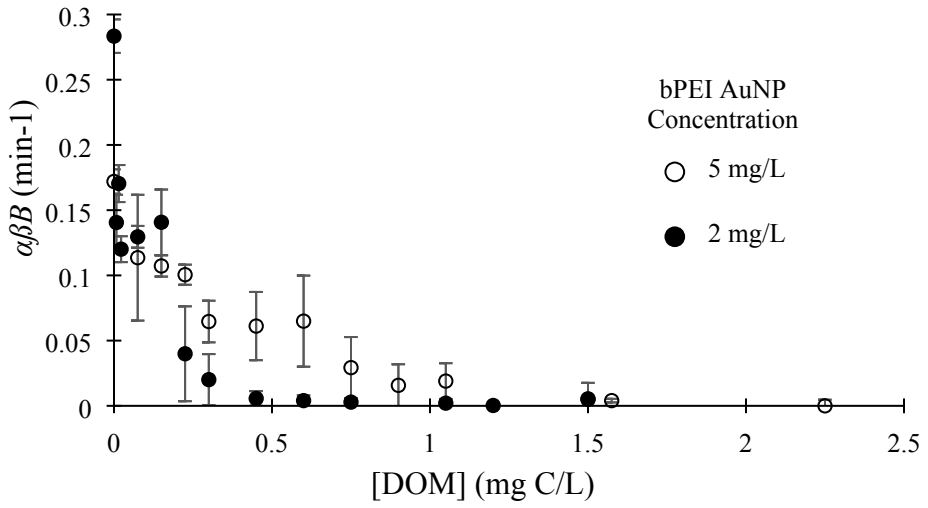


**Figure S14.** Pseudo-first order rate constants (*αβB)* for attachment of bPEI-AuNPs (2 mg/L or 5 mg/L) to glass beads (20 g/L) in 1 mM HEPES, 20 mM NaCl, and varying concentrations of SRNOM. Error bars represent one standard deviation of replicates.

## 12.Loss of bPEI AuNPs to vessel walls

Figure S15 shows the spectra obtained from a batch experiment with 2 mg/L bPEI-AuNPs, 1 mM HEPES, and 20 mM NaCl. The shape of the spectra indicates no homoaggregation but the decreasing absorbance indicates a decrease in NP concentration. This is likely due to the NPs attaching to the vessel walls. From this loss, it is possible to calculate an apparent rate constant in the absence of GBs.

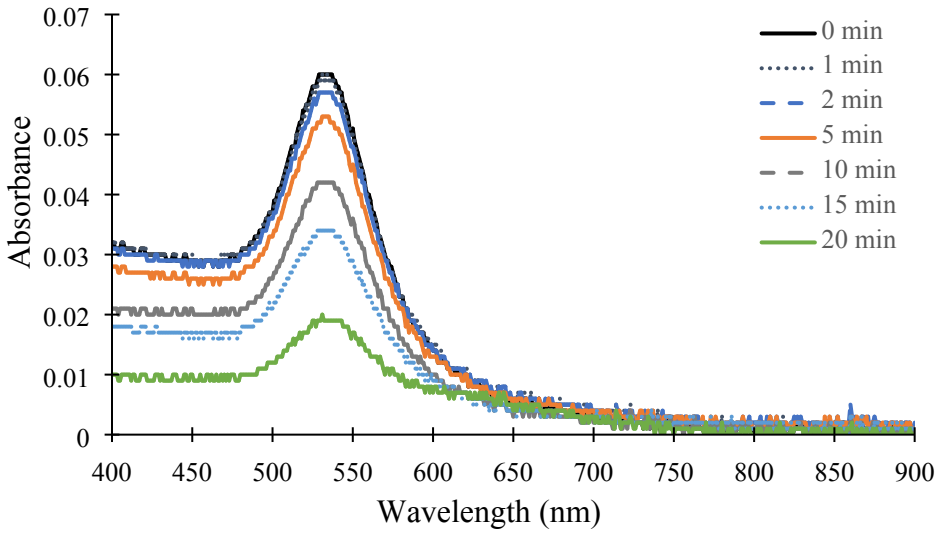


**Figure S15.** Background corrected UV-Vis spectra over time for 2 mg/L bPEI-AuNPs, 0 g/L GB, 20 mM NaCl, 1 mM HEPES, 0 mg C/L SRNOM.

Figure S16 shows the pseudo-first order rate constant in the absence of GBs for varying DOM:ENP ratios. The decrease in the rate constant is consistent with the positively charged bPEI-AuNPs having a higher affinity for the vessel walls than the negatively charged SRNOM-coated ENPs, suggesting that DOM surface coverage is again controlling the attachment efficiency between the NPs and a heterogeneous surface. ENP losses to the vessel walls were incorporated into the conceptual model by assuming that a first order term of the following form described those losses:

$$\frac{dN}{dt} = -\phi\left(\theta_{ENP}\right)\alpha_{ENP-wall}k_{wall}N \qquad \text{(S15)}$$

where $\phi\left(\theta_{ENP}\right)$ is a blocking function dependent on $\theta_{ENP}$, the fraction of the ENP surface coated by DOM; $\alpha_{ENP-wall}$ is the attachment efficiency between the bPEI-AuNPs and the vessel walls; and $k_{wall}$ is the effective first-order collision frequency between ENPs and the vessel walls. Model fits using the two forms of $\phi\left(\theta_{ENP}\right)$ are shown on Figure S16 and demonstrate that attachment to the vessel-walls is well-described by models of this form. For the purposes of this analysis, $\theta_{limit} = 0.83$ (the value determined by the fit of the model to the data in the presence of glass beads), the data collected in the absence of DOM was omitted because it was low relative to values measured with added NOM, and the value

of $\alpha_{ENP-wall}k_{wall}$ was left as a fitting factor and found to be 0.083 $min^{-1}$. It should be noted that these data and this analysis simply confirm the form of the rate equation describing the loss of bPEI-AuNPs to the vessel walls and were not used to "correct" the data measured in the presence of glass beads.

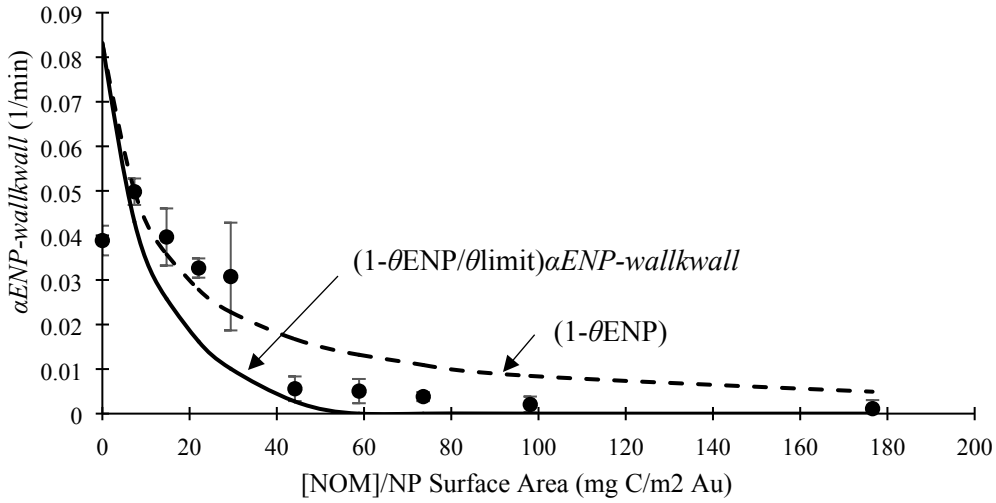


**Figure S16.** Pseudo-first order rate constants ($\alpha_{ENP-wall}k_{wall}$) for apparent removal rate in the absence of GBs. 2 mg/L bPEI-AuNPs, 1 mM HEPES, 20 mM NaCl, varying SRNOM concentrations. Error bars represent one standard deviation of replicates.

## 13. Model Predictions based on $\theta_{ENP}$

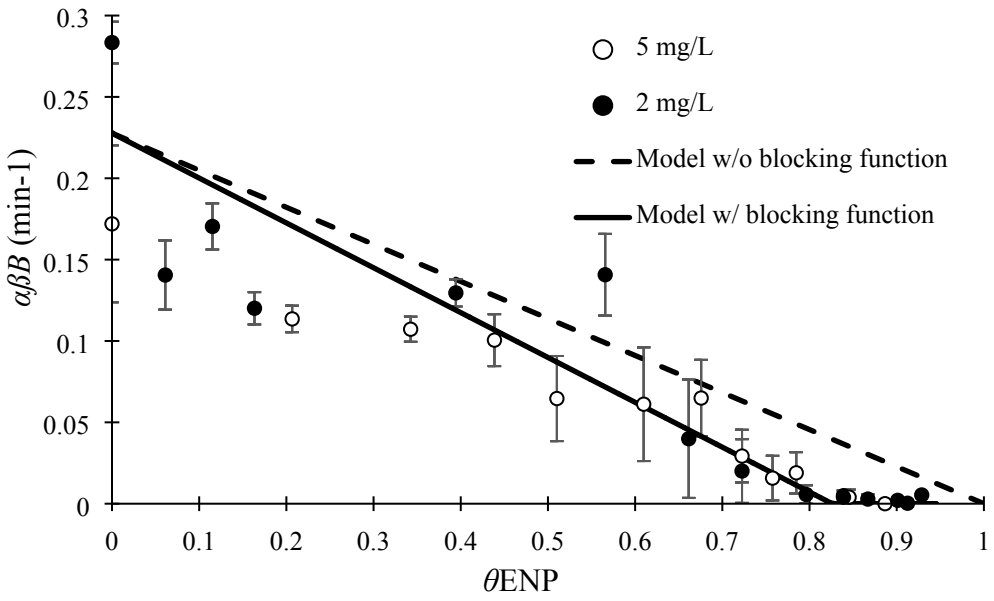


**Figure S17.** Experimentally measured pseudo first-order heteroaggregation rate constants ($\alpha\beta B$) for collisions between bPEI AuNPs and glass beads and comparison with model predictions. 1 mM HEPES, 20 mM NaCl and varying SRNOM concentrations. Error bars represent one standard deviation of replicates.

### References


1. Espinasse, B.; Hotze, E. M.; Wiesner, M. R., Transport and retention of colloidal aggregates of C-60 in porous media: Effects of organic macromolecules, ionic composition, and preparation method. *Environ Sci Technol* **2007,** *41*, (21), 7396-7402.
2. Gonzalez, F. G.; Vilchez, M. A. C.; Hidalgo-Alvarez, R., Adsorption of Anionic Surfactants on Positively Charged Polystyrene Particles .2. *Colloid Polym Sci* **1991,** *269*, (4), 406-411.
3. Surette, M. C.; Nason, J. A., Effects of surface coating character and interactions with natural organic matter on the colloidal stability of gold nanoparticles. *Environ-Sci Nano* **2016,** *3*, (5), 1144-1152.

4. Surette, M. C.; Nason, J. A.; Kaegi, R., The influence of surface coating functionality on the aging of nanoparticles in wastewater. *Environmental Science: Nano* **2019**.
5. Benjamin, M. M.; Lawler, D. F., *Water quality engineering : physical/chemical treatment processes*. John Wiley & Sons: Hoboken, N.J., 2013; p xxv, 878 pages.
6. Turner, A. A.; Rogers, N. M. K.; Geitner, N. K.; Wiesner, M. R., Nanoparticle affinity for natural soils: a functional assay for determining particle attachment efficiency in complex systems. *Environ-Sci Nano* **2020,** *7*, (6), 1719-1729.